Supplementary Information for
Driving Forces for Ultrafast Laser-induced sp^2 to sp^3 Structural Transformation in Graphite

Chenchen Song,[1,2] Mengxue Guan,[1,2] Yunzhe Jia,[1,2] Daqiang Chen,[1,2] Jiyu Xu,[1,2]Cui Zhang,[1,3*] and Sheng Meng[1,2,3*]

These authors contributed equally: Chenchen Song, Mengxue Guan

[1]*Beijing National Laboratory for Condensed Matter Physics and Institute of Physics, Chinese Academy of Sciences, Beijing 100190, China*

[2]*School of Physical Sciences, University of Chinese Academy of Sciences, Beijing 100049, China*

[3]*Songshan Lake Materials Laboratory, Dongguan, Guangdong 523808, China*

[*]*E-mail: cuizhang@iphy.ac.cn; smeng@iphy.ac.cn*

Section I

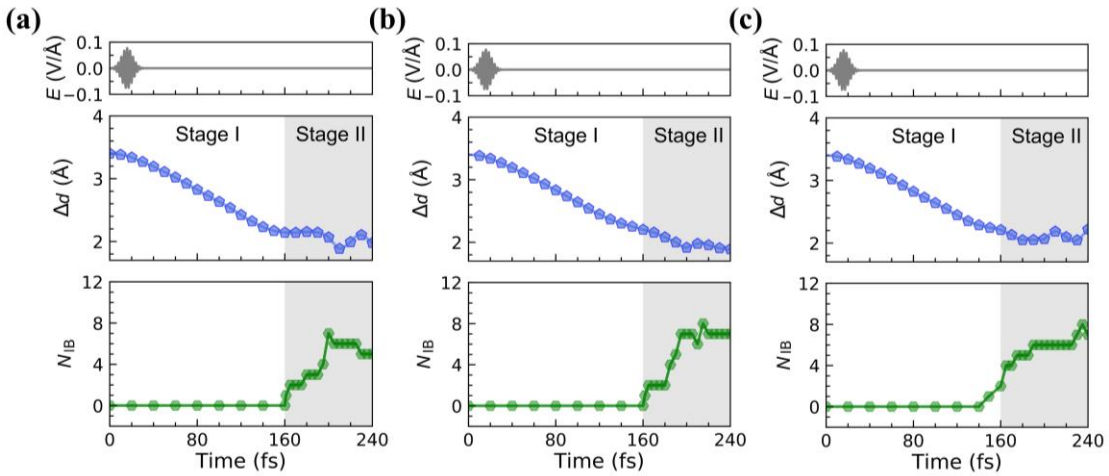

Supplementary Figure 1. (a-c) Three independent simulations initiated with the same laser parameter settings over a random distribution. Time evolution of the laser field waveform, the interlayer spacing Δd and the number of interlayer bonds (N_{IB}) formed in the structural transformation process are shown from top to bottom. The Gaussian-shaped laser pulse is polarized along the armchair direction of graphite with a field strength of $E_0 = 0.077\ \mathrm{V\,Å^{-1}}$ and a fluence of $F = 0.905\ \mathrm{mJ\ cm^{-2}}$. The simulation settings are the same as the main text.

We have performed three different independent simulations initiated with the same laser parameter settings over a random distribution. As shown in Supplementary Figure 1, the light-induced structural transitions occurred in graphite are quantitatively consistent, undergoing stages of rapid interlayer compression (Stage I) and bonding (Stage II). At 160 fs, the interlayer spacing Δd is 2.14, 2.20 and 2.21 Å, respectively, with an ensemble average of 2.18 ± 0.04 Å. Supplementary Figure 1a shows the data reported in the main text (Fig. 1c & 1d).

Section II

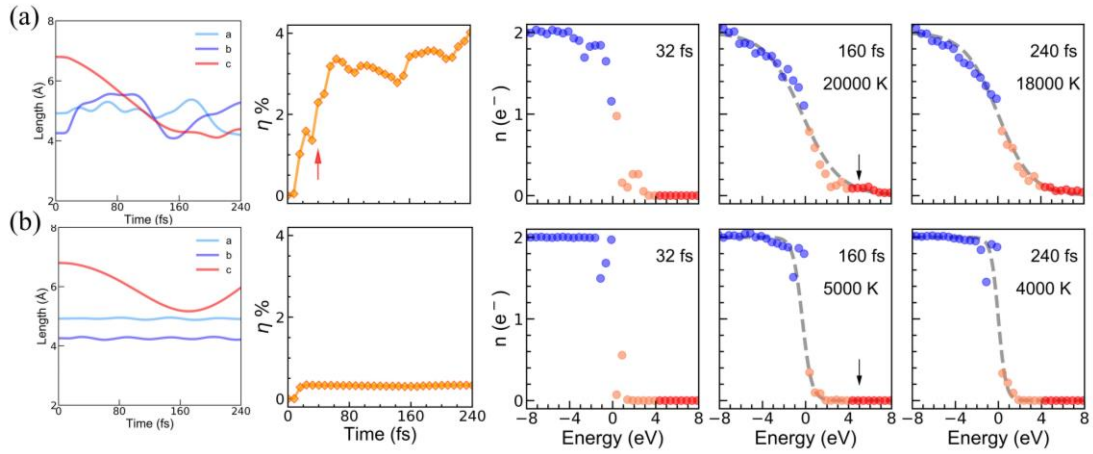

Supplementary Figure 2. Time evolution of the lattice parameters, the percentage of excited electrons (η%) and the electron distributions under laser excitation at a fluence of (a) $F = 0.905$ mJ cm^{-2} and (b) $F = 0.100$ mJ cm^{-2}, respectively. The blue, coral, and red dots are used to present the electron distributions in the energy regions of A, B, and C depicted in the Fig. 4a, respectively. The electronic temperature T_e is obtained by fitting the Fermi-Dirac function (dash lines). The Fermi level E_F is set to 0 eV.

In the case of low-intensity laser irradiation in graphite (lower panel), the lattice length *c* temporarily contracts and then rapidly recovers. For high-intensity laser irradiation where the structure transformation occurs (upper panel), the lattice length *c* undergoes irreversible compression and the lengths of *a* and *b* vibrates under intense irradiation which facilitates the rearrangement of the in-plane atoms.

For the weak photoexcitation without sp^3 bond formation ($F = 0.100$ mJ cm^{-2}), the carrier multiplication effect and high-energy electron scattering are negligible. In contrast, under strong excitation ($F = 0.905$ mJ cm^{-2}), the carrier multiplication is significant, and high-energy electrons are important for driving the out-of-plane distortion and triggering the interlayer bond formation.

Section III

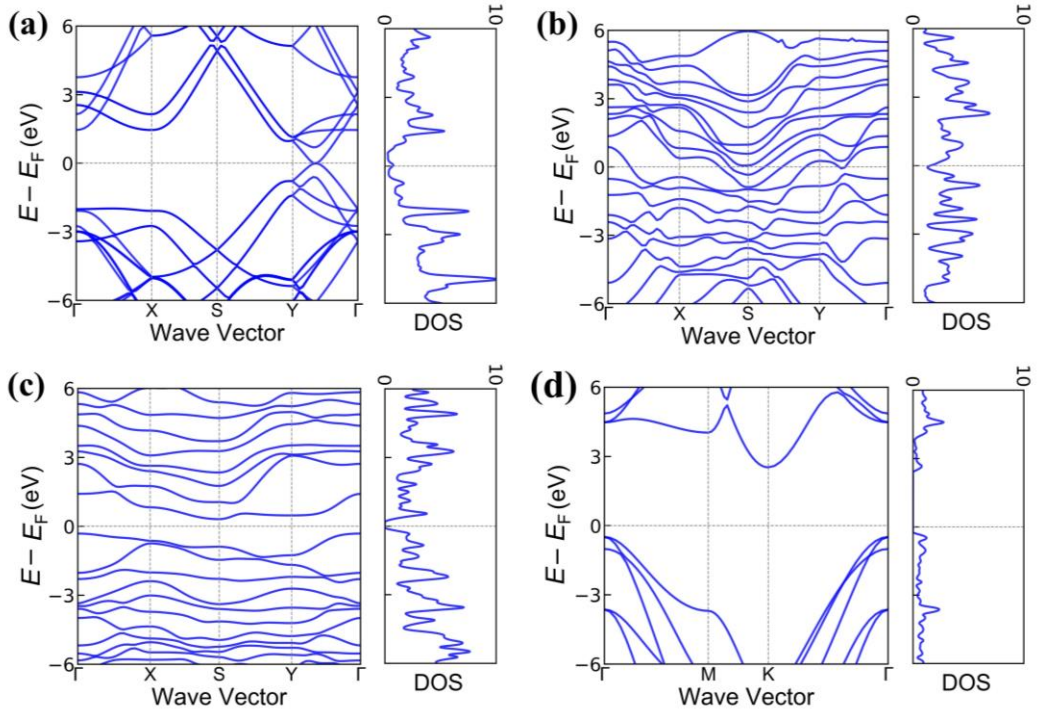

Supplementary Figure 3. Band structure and density of states (DOS) of photoexcited graphite at (a) 0 fs, (b) 160 fs, and (c) 240 fs, respectively. (d) Band structure and DOS of hexagonal diamond.

Section IV

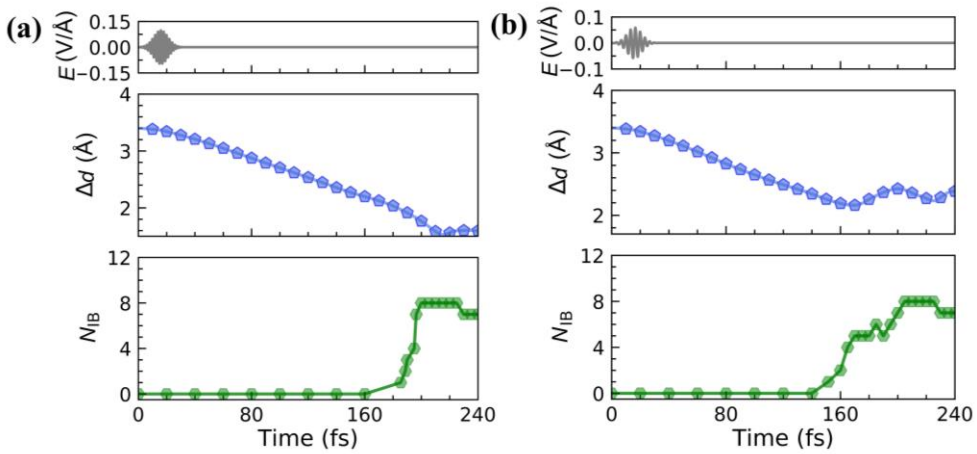

Supplementary Figure 4. Time evolution of the laser field waveform, the interlayer spacing Δd and the number of interlayer bonds (N_{IB}) formed in the structural transformation process under excitation of (a) 600 nm and (b) 1000 nm lasers, respectively. The Gaussian-shaped laser pulse is polarized along the armchair direction of graphite. The field strength of the laser in (a) is $E_0 = 0.098\ \mathrm{V\ Å^{-1}}$. The field strength of the laser in (b) is $E_0 = 0.059\ \mathrm{V\ Å^{-1}}$.

We have also carried out non-adiabatic molecular dynamic calculations of graphite under laser excitation with a wavelength of 600 nm and 1000 nm, respectively, achieving interlayer compression and bonding similar to that of 800 nm, as shown in Supplementary Figure 4. The laser wavelength has no essential effect on the photo-induced sp^2-sp^3 bond transition in graphite. However, for lasers with shorter wavelengths, higher electric field strengths are more favorable for the structural transformation.

Section V

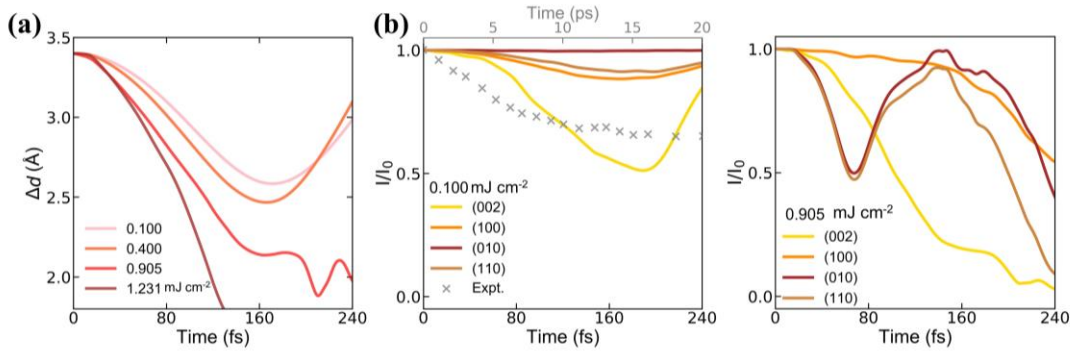

Supplementary Figure 5. (a) Time evolution of the graphite interlayer spacing Δd at different laser fluences. Laser pulses have a photon energy of 1.55 eV and a maximum field intensity E_0 ranging from 0.026 to 0.077 V Å^{-1} at 16 fs. (b) Diffraction intensities of (002), (100), (010), and (110) planes in graphite at a laser fluence of 0.100 mJ cm^{-2} and 0.905 mJ cm^{-2}, respectively. The dotted line represents the time evolution of (008) diffraction intensity reported in the experiment (apparent laser fluence: 21mJ cm^{-2}), where no interlayer bonds are formed.[1]

We compare in Supplementary Figure 5 the time evolution of the interlayer spacing Δd and diffraction intensity I/I_0 of photoexcited graphite obtained from experiments and simulations for different laser fluences. Simulated results show the phenomena of interlayer contraction in graphite after photoexcitation at a certain level of laser fluences. We note that the interlayer contraction is rapid and dramatic, which is attributed to the model and conditions chosen in the simulations. Moderately small graphite supercell used in the constant-pressure-energy (NPE) ensemble, lacking strict boundary constrains, and the direct action of the laser pulse on the interior of lattice may result in faster and more sensitive responses of graphite. We reveal the microscopic short-time non-equilibrium behavior in a small domain where the laser-induced phase transition occurs, rather than the macroscopic long-time steady-state phenomena detected in experiments.

In addition, our simulation results indicate that strong laser pulses accelerate the reduction of interlayer spacing and low-intensity excitations lead to only a temporary interlayer contraction followed by a spacing recovery. Only when the laser intensity is high enough, the interlayer spacing can be irreversible compressed, which facilitates

the formation of interlayer bonds. When the simulation laser fluence is as high as $F = 1.231$ mJ cm^{-2}, the graphite structure tends to be disordered, so we regard this value as the calculated damage threshold F_c. It is clear the laser intensity capable of initiating the phase change is close to the damage threshold of graphite. Similar results have been observed in experimental studies where laser fluences approaching to the damage threshold can drive the formation of interlayer bonds in graphite.[1] We note that the damage threshold estimated here is much smaller than the experimental value (77 mJ cm^{-2}), mainly because the light field applied in the calculation acts uniformly on the interior of the material without light reflection and electronic screening. It is thus not appropriate to directly compare the apparent laser fluence used in the experiments and the interior laser fluence within materials adopted in the simulations.

The nonequilibrium phonon dynamics can be observed experimentally by monitoring the intensity evolution of the Bragg peak using the ultrafast electron diffuse scattering (UEDS) tools.[2,3] The structural distortion is related to the diffraction intensity $I(t)$ through the Debye-Waller formula,

$$I = I_0 \exp[-\langle |\mathbf{q} \cdot \mathbf{u}|^2 \rangle] \quad (7)$$

where $\mathbf{u}$ is the displacement vector of an atom from its original position at $t = 0$, $\mathbf{q}$ is the reciprocal lattice vector of the probed reflection, and the brackets $\langle\ \rangle$ denote an average over all atoms in the supercell.

Supplementary Figure 5b show the diffraction intensity variation of photoexcited graphite for several different lattice plane families, compared to the experimental measurements. Under weak excitation that fails to yield interlayer contraction in graphite, the diffraction intensity of (100), (010) and (110) Bragg peaks varies very little and in contrast, the intensity of (002) show a transient decay. Similar decay behavior of the diffraction intensity in photoexcited graphite has been reported in experimental work,[1] as shown in Supplementary Figure 5b. With a high laser fluence capable of yielding interlayer compression of graphite, the intensities of all Bragg peaks

show significant oscillations and continuous decay due to the irreversible changes of interlayer spacing and sp^3 bond formation.

REFERENCES

1 Raman, R. K. et al. Direct observation of optically induced transient structures in graphite using ultrafast electron crystallography. *Phys. Rev. Lett.* **101**, 077401 (2008).

2 de Cotret, L. P. R. et al. Time-and momentum-resolved phonon population dynamics with ultrafast electron diffuse scattering. *Phys. Rev. B* **100**, 214115 (2019).

3 Stern, M. J. et al. Mapping momentum-dependent electron-phonon coupling and nonequilibrium phonon dynamics with ultrafast electron diffuse scattering. *Phys. Rev. B* **97**, 165416 (2018).